Lead transition metal oxides: Globally alike, locally very diverse

A. Bussmann-Holder [1], A. M. Glazer [2], A. Majchrowski [3], I. Lazar [4], A. Soszyński [4], and K. Roleder [4]

[1] *Max-Planck Institute for Solid State Research, Heisenbergstrasse 1, D-70569 Stuttgart, Germany*

[2] *Clarendon Laboratory, University of Oxford, Oxford OX1 3PU, United Kingdom*

[3] *Institute of Applied Physics, Military University of Technology, ul. Kaliskiego 2, 00–908 Warsaw, Poland*

[4] *Institute of Physics, University of Silesia, ul. 75 Pułku Piechoty 1, 41–500 Chorzów, Poland*

(Received 22 December 2025; revised 25 February 2026; accepted 21 May 2026; published 15 June 2026)

The lead transition metal oxides $PbTiO_3$, $PbZrO_3$, and $PbHfO_3$ are shown to be extremely similar in their overall properties, such as soft-mode behavior, phase transitions, and long-wavelength related characteristics. However, locally, they develop very different qualities because, as the BO_6 mass increases (where B ≡ Ti, Zr, Hf), the anharmonicity of each compound increases significantly, leading to the formation of intrinsically localized modes (ILMS) or discrete breathers (DBS). This explains their exceptionally flat transverse acoustic modes. These nonlinear excitations are observed in birefringence measurements, where their coexistence with the phonon spectrum is demonstrated. While the soft modes, whether normalized by mass or temperature (long-wavelength optic and zone boundary acoustic modes), follow nearly identical temperature dependencies, the transverse acoustic modes exhibit a highly dispersion-free momentum dependence, characteristic of ILMS or DBS. Crucially, our findings support the earlier notion that the unusual dynamics are solely due to the BO_6 polarizable unit, with the Pb subarrays acting merely as spectators. Furthermore, these results provide a unique explanation for the appearance of the transient phase below the phase transitions of $PbZrO_3$ and $PbHfO_3$, which appears to be intrinsic to these two compounds.

DOI: 10.1103/4dlq-9mb1

I. INTRODUCTION

The three lead perovskite oxides, $PbTiO_3$ (PTO), $PbZrO_3$ (PZO), and $PbHfO_3$ (PHO), are well-investigated compounds because of their multiple applications and technological importance, such as in piezo-actuators and ferroelectric random-access memories [1]. Also, from a scientific point of view, they have all been thoroughly investigated, including their mixed transition metal compounds. $PbTi_{1-x}Zr_xO_3$, especially, has been the focus of research early on because its Curie temperature can be tuned by almost 300 K, thereby shifting its excellent piezoelectric properties to the desired temperature scale [2]. All three compounds are cubic at high temperatures and undergo a structural phase transition to either a ferroelectric (PTO) [3] or antiferroelectric (PZO, PHO) [4,5] phase. While PTO has long been considered to exhibit the prototypical displacive phase transition driven solely by a long-wavelength transverse soft optic mode, PZO and PHO have been taken as textbook examples of antiferroelectricity [6]. These points of view have, however, to be abandoned with more intensive and refined experimental techniques, showing that PTO also shows order-disorder characteristics [7] whereas PZO and PHO follow a complicated phase transition sequence with partially unknown and unresolved structures [4,8–13]. Common to both is the appearance of a transient phase below their Curie temperatures, which vanishes rapidly with decreasing temperature. Recently, a novel, almost hidden low-temperature phase has been discovered, which shows polar (ferroelectric-like) properties [14–16].

The mutual features of the three compounds are, besides their high-temperature cubic phase, their Pb framework. While in related perovskite cubic oxides such as $BaTiO_3$, $SrTiO_3$, and $CaTiO_3$, the A-site (in ABO_3) cationic substructure primarily determines the unit cell size and functions as a rigid ion with no charge overlap with the oxygen or transition metal ions [17], the role of Pb is quite different. Its lone-pair configuration forms covalent bonds with oxygen and transition-metal ions [18]. This difference in the various transition metal oxides has been taken as evidence that Pb^{2+} is the essential structural driver of the ferro- or antiferroelectric properties, since the 2s ions of lead form strongly directional bonds. Notably, it has been observed that the lone pairs in PZO and PHO order in an antiparallel array, which suggests that this is the source of antiferroelectricity in these compounds [10,19–21].

II. THEORETICAL MODELING

However, in a variety of recent publications based on the polarizability model [22–25] and experimental data, we have demonstrated that the BO_6 subunit in ABO_3 perovskites is the decisive one, rather than the lead framework, and highlight this in the following. Within the polarizability model,

Published by the American Physical Society under the terms of the Creative Commons Attribution 4.0 International license. Further distribution of this work must maintain attribution to the author(s) and the published article's title, journal citation, and DOI. Open access publication funded by Max Planck Society.

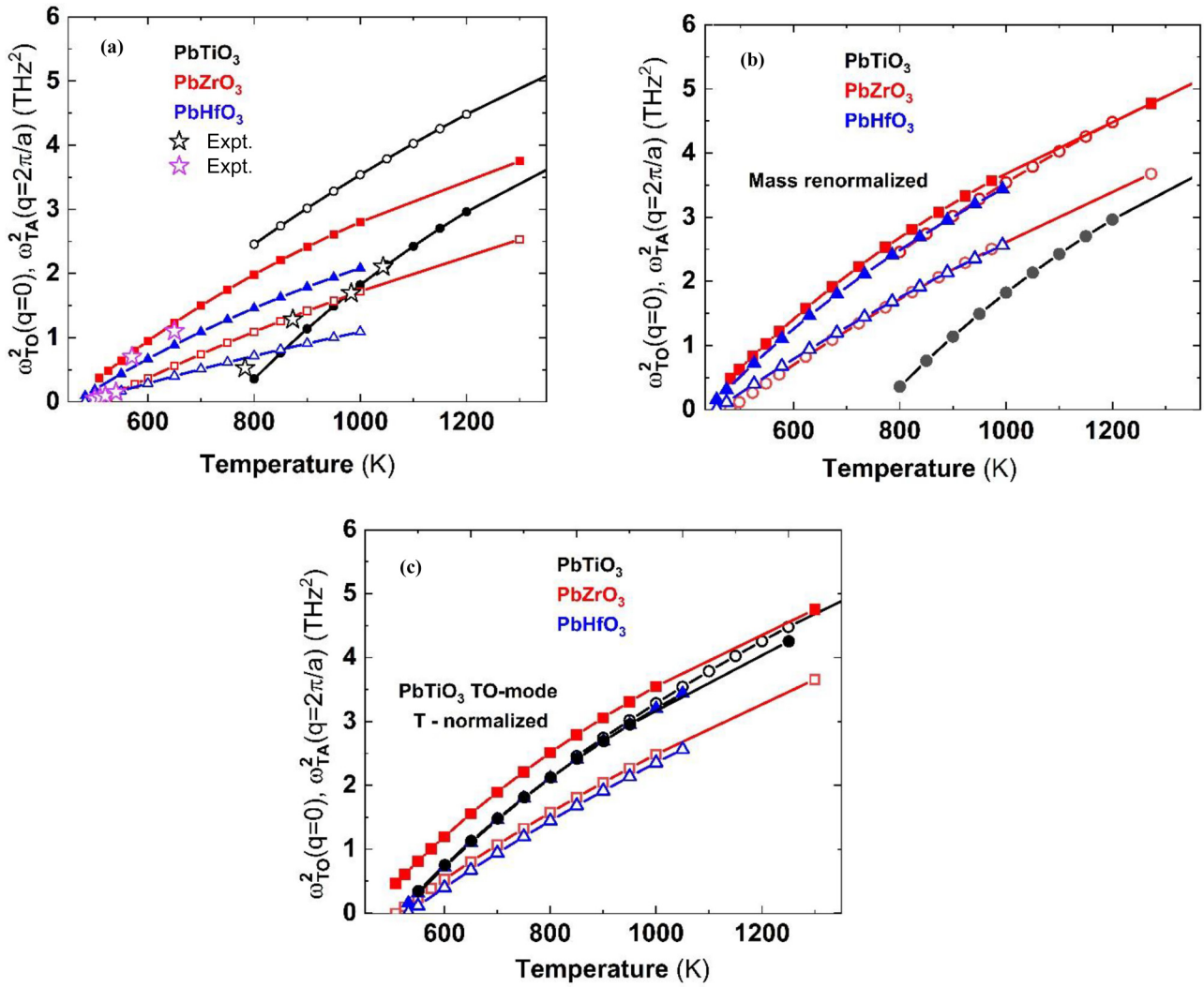


FIG. 1. (a) Temperature dependence of the squared TO (full symbols) and TA (open symbols) modes for PTO (black), PZO (red), and PHO (blue) modes. Open black (PTO) and blue (PHO) refer to experiments of Refs. [28,29], (b) the same as in (a); however, with the modes renormalized by the mass, as explained in the text, and (c) the same as in (b), with the temperature scale for the TO mode of PTO being shifted by 300 K.

this structural subunit is described as a nonlinearly polarizable entity surrounded by its electronic shell. The coupling between the core and the shell is given by an attractive harmonic one g_2 and a repulsive stabilizing anharmonic term g_4 which taken together define a double-well potential in the relative core-shell displacement coordinate w, given by $V(w) = g_2 w^2 + g_4 w^4$. In the equations of motion the fourth-order term appears as a cubic term in w which typically is approximated within the self-consistent phonon approximation (SPA) by its pseudo-harmonic form: $g_4 w^3 = 3g_4\langle w^2\rangle w$ to yield together with the harmonic term a temperature dependent coupling: $g_T w = (g_2 + 3g_4\langle w^2\rangle)w$. The temperature dependence of the modes is thereby exclusively determined by g_T with $\langle w^2\rangle$ being evaluated self-consistently. Based on this model, the two soft modes, namely long-wavelength transverse optic TO and zone-boundary transverse acoustic TA, observed in each of the three systems are consistently and in agreement with experimental data described. Note that the soft TA zone boundary mode relates to the oxygen octahedral rotation and yields the tilting of this at the phase transition temperature in analogy to $SrTiO_3$ [26]. In addition, we have emphasized that the mass of the polarizable unit BO_6 causes the difference in the three compounds. In Fig. 1(a) the already published temperature dependence of the squared frequencies $\omega^2_{\mathrm{TO}}(q=0)$, $\omega^2_{\mathrm{TA}}(q=2\pi/a)$ is shown together with experimental data where available [27]. While $\omega^2_{\mathrm{TO}}(q=0)$ is proportional to $1/\mu$ where μ is the reduced unit cell mass, $\omega^2_{\mathrm{TA}}(q=2\pi/a)$ is proportional to $1/m_1$ where m_1 is the polarizable cluster mass, i.e., TiO_6, ZrO_6, HfO_6, respectively. The overall temperature dependence of these modes of the three compounds PTO, PZO, PHO [Fig. 1(a)] shows little analogies between them, but if m_1 is mass-renormalized to PTO like $m_1(ZrO_6)/m_1(TiO_6)$ and similarly for PHO, this picture changes to Fig. 1(b), where the TO modes of PZO and PHO now overlap with the TA mode of PTO. In addition, the related TA modes of the mass-renormalized PZO and PHO perovskites follow almost an identical temperature dependence. This finding strongly supports our notion of "mass matters" [27] and the conclusions that the essential unit of the perovskites is represented by the polarizable mass. A

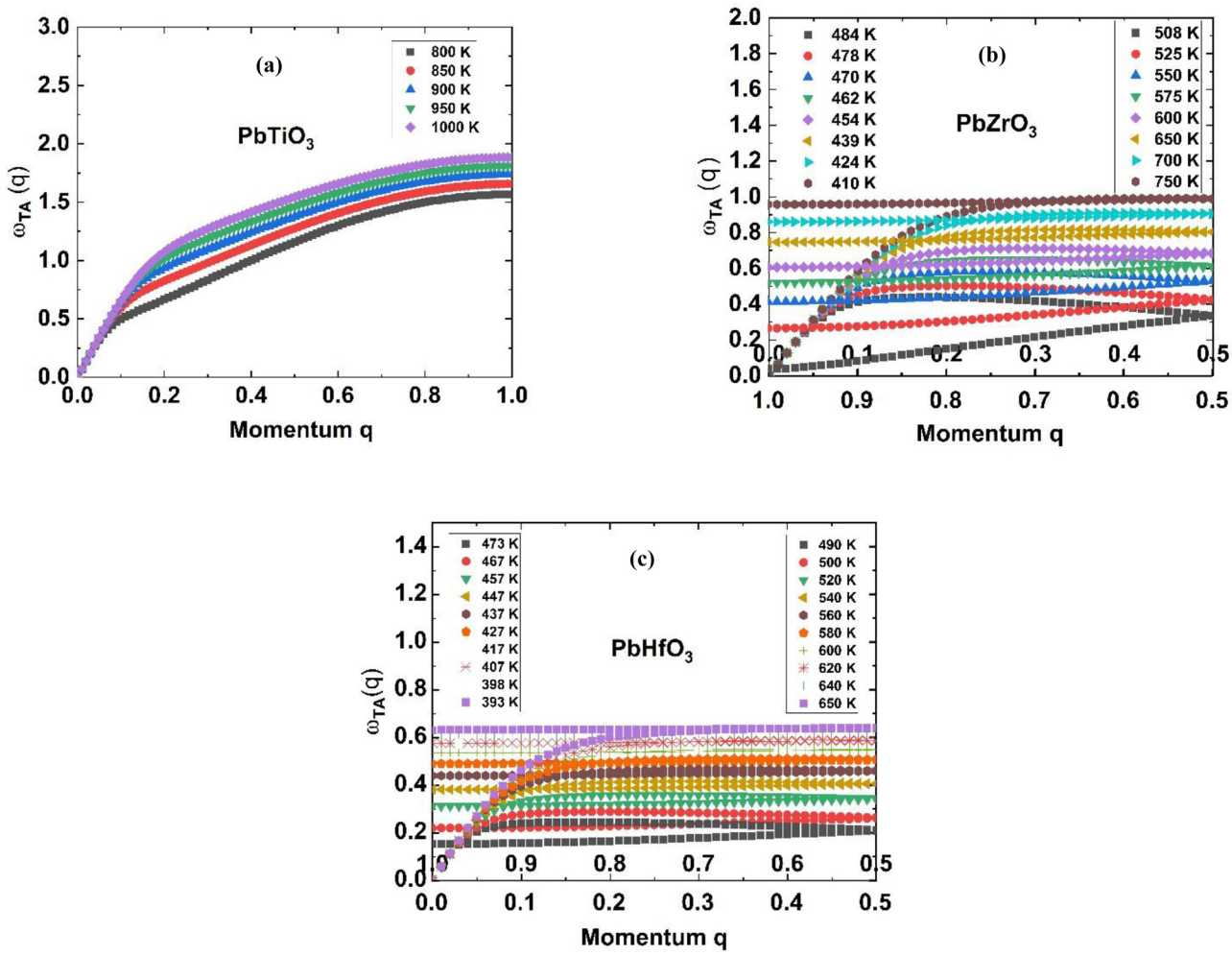


FIG. 2. The transverse acoustic mode as a function of temperature and momentum q for (a) PTO, (b) PZO, and (c) PHO. Note that in (a), backfolding of the mode is meaningless, while in (b) and (c), the modes are backfolded from q = 0.5 to the zone center as expected for temperatures below their transition temperature T_C, with energies increasing with decreasing temperature below T_C. The temperatures are given in the figures, where for $T < T_C$ the temperatures have been extracted from the Landau law.

remarkable finding is that the roles of TA and TO modes are interchanged, namely, the TO modes of PZO and PHO follow the TA mode temperature dependence of PTO, which favors the speculation that these modes are inherently acoustic modes. In Fig. 1(b), the TO mode of PTO splits off from the remaining modes since its softening takes place at substantially enhanced temperatures. In view of this "anomalous" behavior, we have renormalized it by temperature T-300 K to find common features with the other modes. This is shown in Fig. 1(c), where amazingly the PTO's TO mode now coincides with its related TA mode and the remaining TO modes of PZO and PHO.

The remarkable results of the renormalization procedure, as shown in Fig. 1(c), reveal that four out of six modes follow nearly identical temperature dependences, while the remaining two TA modes of PZO and PHO are almost degenerate. Firstly, it shows that the PTO-related TA mode is driven by the same polarizability coordinate as its TO mode, a phenomenon already observed in $SrTiO_3$ [26]. Secondly, the TO modes of PZO and PHO suggest an inherent tendency towards a ferroelectric state, which has recently been confirmed at lower temperatures [15,16]. Overall, these impressive outcomes demonstrate that all lead transition metal oxides share common features in their dynamical properties.

By comparing the momentum q-dependent transverse acoustic modes of the three systems (Fig. 2), it is very striking that large differences in their dispersions are visible. While that of PTO [Fig. 2(a)] can still be understood on the basis of a Debye-type model and folding back of the TA mode is meaningless, both PZO [Fig. 2(b)] and PHO [Fig. 2(c)] TA phonon modes exhibit dispersion-free behavior from approximately q = 0.25, which has also been observed experimentally [30], and which is temperature dependent and increases with increasing temperature. Note that this could experimentally be related to incommensurations speculated to appear in PHO [31]. Beyond this, the flat modes are reminiscent of a van Hove singularity, which has been discussed as the origin of flat bands [32,33]. As the temperature decreases, these phonons soften at $q = 2\pi/a$ and drive the transition to the antiferroelectric, transient ferroelectric state associated with octahedral tilting. The consequences of this transition are that the modes fold back to the zone center below their

transition temperature and adopt a zone-center TO mode character, which increases in energy with decreasing temperature [34]. In addition, the new TO modes exhibit no dispersion, i.e., they are completely flat with an extremely high density of states in ω space. Besides PZO and PHO, related features have been observed in glasses and disordered solids, and have been interpreted in terms of van Hove singularities or boson peaks [35–37]. Another approach is adopted here in terms of huge anharmonicity related to g_4, where inherent solutions to the above applied polarizability model and beyond the SPA are shown to be the basis for intrinsically localized modes (ILM) and discrete breathers (DB) [38–40]. Specifically, for various perovskite oxides, it has been demonstrated that ILM and DB formation can be the origin of relaxor behavior [41–43], as this is a prerequisite for the site-dependence of the local double-well potential, which enables the dispersion-free mode. The formation of ILMs or DBs is favored by the Φ_4-type potential introduced above; however, instead of using the SPA, exact solutions of this potential are searched for, where in the equations of motion, the third-order term in w is not replaced by its pseudo-harmonic average, but exact solutions to the nonlinear equations of motion are searched for. In order to derive these, the displacement coordinates of ion 1 with mass m_1, ion 2 with mass m_2 and shell (treated in the adiabatic approximation) u_{1n}, u_{2n}, w_{1n} are assumed to be time-periodic like:

$$u_{1n}(t) = A\xi_{1n}\cos(\omega t)$$

$$u_{2n}(t) = B\xi_{2n}\cos(\omega t)$$

$$w_{1n}(t) = C\eta_{1n}\cos(\omega t)$$

with amplitudes A, B, C, respectively and ξ, η the corresponding displacements. The amplitudes are derived through the equations of motion and are frequency-dependent, and the electronic shells are treated in the adiabatic limit. Analytical solutions to the equations of motion are obtained by using the rotating wave approximation [44], namely:

$$\cos^p(\Theta) = \frac{p!}{2^{p-1}}\sum_{k=1}^{p}\frac{\cos(k\Theta)}{\left[\frac{p+k}{2}\right]!\left[\frac{p-k}{2}\right]!} \qquad p,k \equiv \text{odd},$$

$\cos^{r-1}(\omega t) = C_r\cos(\omega t) + higher\ \ harmonics$ and $\mathrm{r} = 4$ yielding $C_r = 3/4$. Momentum-independent frequencies as observed in PZO and PHO are achieved by the ansatz $w = -2u$. This choice for ILM's odd parity displacement patterns requires that at site $n = 0$ a dipole moment with "length" n_c (displacement ξ_0) is formed, which is compensated by the surrounding ordered structure by creating at site n counted from n_c a dipole moment in the opposite direction with displacement ξ_n according to $\xi_n = \xi_0 - \frac{n}{2}: \ \ n \equiv \text{even};\ \ \xi_n = -[\xi_0 - \frac{n}{2}]: \ \ n \equiv \text{odd}$. This choice guarantees that at atomic site n_c the breather spatial extensions have reached their limit. Thus, the extension of the DB depends on the magnitude of the central dipole moment and two solutions of ω result, which need to be the same over all sites of the breather extent until n_c is reached [38]: The frequencies for the above considered type of displacement pattern (introducing the definition

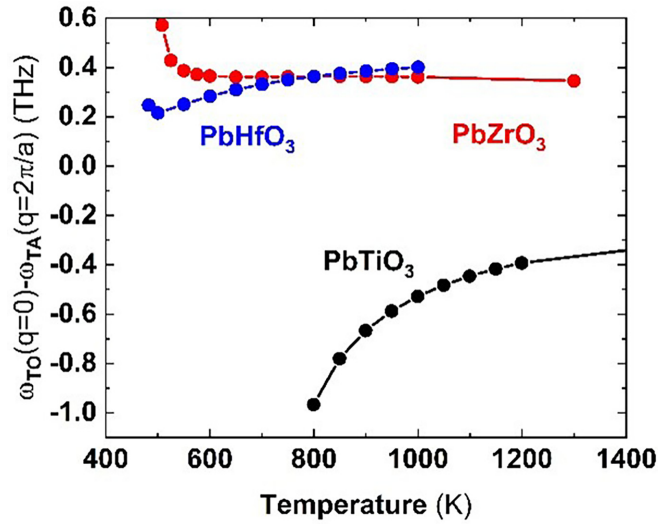


FIG. 3. Existence regime Δ of the DB or ILM formation for PTO, PZO, and PHO.

$(g = 2g_2 + 3/4\tilde{g}_4C^2)$ are at site $n = 0$:

$$\omega_1^2 = \frac{1}{m_1}\left[4f' + g\frac{C}{A}\right] - \frac{2f'}{n_c m_1} \tag{1}$$

$$\omega_2^2 = \frac{2f}{m_2}\left[1 - \frac{1}{n_c}\frac{1}{2 + \frac{gC}{f(2C-A)}}\right] \tag{2}$$

where f and f' are the nearest and second neighbor couplings. At all other sites the solutions are $\omega_1^2 = \frac{1}{m_1}[4f' + g\frac{C}{A}]$ and $\omega_2^2 = \frac{2f}{m_2}$. The solutions Eq. (1), (2) are only stable as long as they are lying in the optic-acoustic mode gap Δ (see Fig. 3), which applies only to the acoustic type mode Eq. (1), whereas the optic type mode lies above the SPA spectrum and can be discarded. The envelope function of the ILM/DB-related displacements can be well approximated by $1/\cosh(n)$ and $-1/\cosh(n)$. This is true only for the case that g_4 becomes site-dependent n like: $\tilde{g}_4^{(n)} = g_4/2(n - n_c)^2$. It implies that the double-well potential varies within the breather region from site to site, being steep and broad in the breather center and becoming smoother with increasing n, to be pseudo-harmonic for distances further apart. Correspondingly, for large $\tilde{g}_4^{(n)}$, the shell, i.e., the electron, is far apart from its core and delocalizes over the breather spread, whereas in the opposite limit it becomes completely localized. This corresponds to a situation where covalent and ionic bonding coexist. The TA-type mode emerging from the above approach is completely flat, and in order to guarantee its existence, it is confined to the gap between the SPA TA and TO modes, which limits its stability region. Clearly, the SPA TA modes have their largest energies at the zone boundary, whereas the smallest values of the SPA TO modes are at the zone center. Thus, the gap $\Delta = \omega_{\mathrm{TO}}(q = 0) - \omega_{\mathrm{TA}}(q = \frac{2\pi}{a})$ defines the possible existence region of ILM or DB solutions. An additional condition for DB, ILM formation is related to ω_1^2 from the inequality condition: $\frac{2fg_T}{2f+g_T} < g_T\frac{C}{A} < \frac{\frac{2fg_T}{2f+g_T}(m_1+m_2)}{m_2} - 4f'$. This concerns the mass ratio, the elasticity proportional to f' and the lattice stability as determined by $\frac{2fg_T}{2f+g_T}$, all of which guarantee the

existence regime of DB or ILM formation. The mass ratio indicates that the larger the polarizable cluster mass and the smaller the rigid ion mass are, the more the stability region increases. Further, the softer the system is (f' denotes the elastic energy), the broader is the energy window for DB's. The structural stability should be robust, i.e., g_T is finite.

The results for Δ are shown in Fig. 3 and provide evidence of the large difference between PTO and PZO, PHO, respectively.

In PTO, ILM, or DB formation can clearly be excluded from taking place, since the TA mode has higher frequencies than the TO mode, and a gap is absent. PZO and PHO are distinctively different: both show finite values for the differences and exhibit almost identical values for increasing temperature. Close to their phase transition temperatures, Δ appears to increase and almost diverge. Since the DB or ILM solutions coexist with the regular modes, a superposition of both displacements is made, namely:

$$\begin{aligned} & g_2(w_{1n,\mathrm{SPA}} + w_{1n,\mathrm{breather}}) + g_4(w_{1n,\mathrm{SPA}} + w_{1n,\mathrm{breather}})^3 \\ &= g_2 w_{1n,\mathrm{SPA}} + g_4 w_{1n,\mathrm{SPA}}^3 + 3g_4 w_{1n,\mathrm{breather}}^2 w_{1n,\mathrm{SPA}} \\ &\quad + g_2 w_{1n,\mathrm{breather}} + g_4 w_{1n,\mathrm{breather}}^3 + 3g_4 w_{1n,\mathrm{SPA}}^2 w_{1n,\mathrm{breather}} \\ &= \left(g_T + 3g_4 w_{1n,\mathrm{breather}}^2\right) w_{1n,\mathrm{SPA}} \\ &\quad + \left(g_T + g_4 w_{1n,\mathrm{breather}}^2\right) w_{1n,\mathrm{breather}} \end{aligned}$$

with indices *breather* and *SPA* referring to either of the chosen displacements. These combined displacements add a temperature dependence to the DB, ILM solution through g_T and nonlinearity to the ordinary phonon modes through the term $g_4 w_{1n,\mathrm{breather}}^2$. Even in the case $g_T = 0$, i.e. at the phase transition, the coupling to the breather prevents a freezing of any soft mode. This enlarges the DB existence regime. Conversely, the breather adopts a temperature dependence since g_2 is replaced by g_T, which renormalizes its potential from hard-core ($g_2 < 0$) to soft ($g_T > 0$). This ansatz has the consequence that the dynamical interplay between the regular structure and the locally distorted regions manifests as strongly enhanced diffuse scattering as, e.g., observed in relaxor ferroelectrics. Ghost modes, especially, may be observed to take away spectral weight from the regular modes at certain wave vectors as defined by the DB spatial extent. The real-space patterns of the combined displacements are shown in Fig. 4.

The ILM/DB is at the origin of the structural site $n = 0$ and extends over approximately 18 sites (in the case of Fig. 4). The center defines the dipole "length" n_c. The surrounding DB-modified plane-wave solution corresponds to a fluctuating dipole region at the DB center with a charge transfer region followed by the regular lattice spectrum. The breadth of the DB solution is determined by the onset momentum of the dispersion-free mode, which—as mentioned above—is temperature dependent and moves with decreasing temperature towards the long-wave length limit (see Fig. 2). While the situation in Fig. 4 corresponds to temperatures $T \gg T_C$, in Fig. 5 the temperature is lowered and approaches T_C. As a consequence, the spatial extent of the DB enlarges and fluctuating polar clusters of different sizes appear. These disappear once the gap in the modes vanishes, which happens since

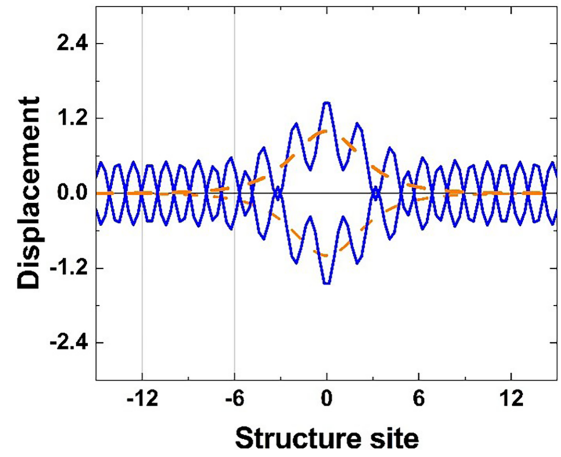


FIG. 4. Real-space displacement pattern of the DB solution (orange) and the combined DB and regular mode (blue). The DB is at the origin (structure site 0) of the structure.

the backfolded optic-like DB mode increases rapidly with decreasing temperature. This defines a regime of coexistence of antiferroelectric and fluctuating polar states, here ascribed to the transient ferroelectric phase below T_C. It is important to note that in a series of previous publications, we have identified precursors to the phase transition in many perovskite oxides. These are here clearly ascribed to the DB formation and thus clarify their microscopic origin. The transient "ferroelectric" type phases of PZO and PHO have been observed for temperatures ≈20 K and ≈35 K below T_C, respectively, and in view of the above scenario, their symmetry is difficult to determine because of the coexistence of the SPA and DB modes, which is in agreement with experiments [8,11].

III. EXPERIMENTAL

Experimentally, DB's or ILM's have been observed mostly in relaxor ferroelectrics [40–42] since the site-dependent double-well potential induces a frequency-dependent dielectric response, which is a signature of our model. However, more recently, new impressive birefringence experiments in the transient phase of PHO have been performed where the coexistence of DB's with the regular phonon modes is undoubtedly visible. Prior to these experiments, the transient phase has been identified by dielectric susceptibility ε measurements on a single crystal of PHO (Fig. 6), where the phase transition around $T_C \approx 500$ K appears as a peak in ε. Below this peak, a strongly size-reduced anomaly in ε appears as a rather flat plateau which vanishes approximately 40 K below T_C. This plateau is a rather indirect signature of DB/ILM formation; yet, it is incompatible with a typical structural phase transition where the dielectric susceptibility would abruptly drop down to the value below 433 K. A clearer picture emerges from birefringence measurements since this is an extremely sensitive tool to observe symmetry changes. In addition, it enables the observation of coexistence regimes of different symmetries through the optical indicatrix orientation, which should adopt specific symmetry-dictated orientations. It is such a unique tool to verify the theoretical expectations. To verify these, we have investigated $PbHfO_3$

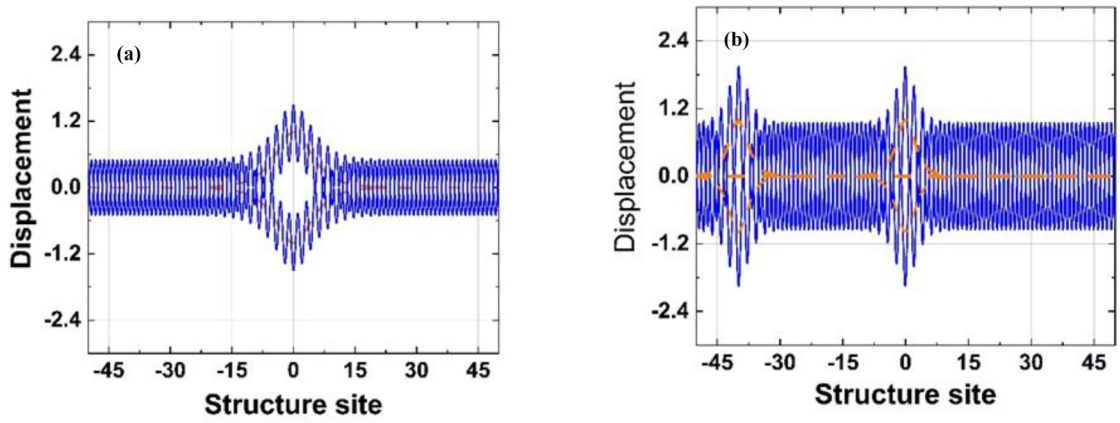


FIG. 5. (a) Pictorial view of combined fluctuating polar clusters and atom displacements for a single DB and (b) for two DB solutions with different spatial extents, both close to T_C.

and $PbZrO_3$ single crystals, in which the existence of an intermediate phase below T_C is clearly visible. The existence of this phase has been debated for decades, especially in $PbZrO_3$, but not in $PbHfO_3$. The temperature dependence of the permittivity for a single $PbHfO_3$ crystal is presented in Fig. 6, where a clear anomaly in ε(T) runs is visible on cooling and heating, indicating also a thermal hysteresis.

A single $PbHfO_3$ and $PbZrO_3$ crystal, both oriented [100], with respective thicknesses of 90 and 87 μm, was used in optical studies to examine the orientation of the optical indicatrix of the regions appearing inside the intermediate phase (see Figs. 7–9). The measurements were performed by means of an Oxford Cryosystems Metripol Birefringence Imaging System (Metripol) described earlier in detail in several articles [45]. The crystal was contained within a Linkam THMS600E temperature microscope stage, which could control temperature to within 0.1 K. The application of our experimental technique enabled us to observe optical indicatrix orientations by measuring the extinction angle φ. This extinction angle is defined for subsequent symmetries and is thus a

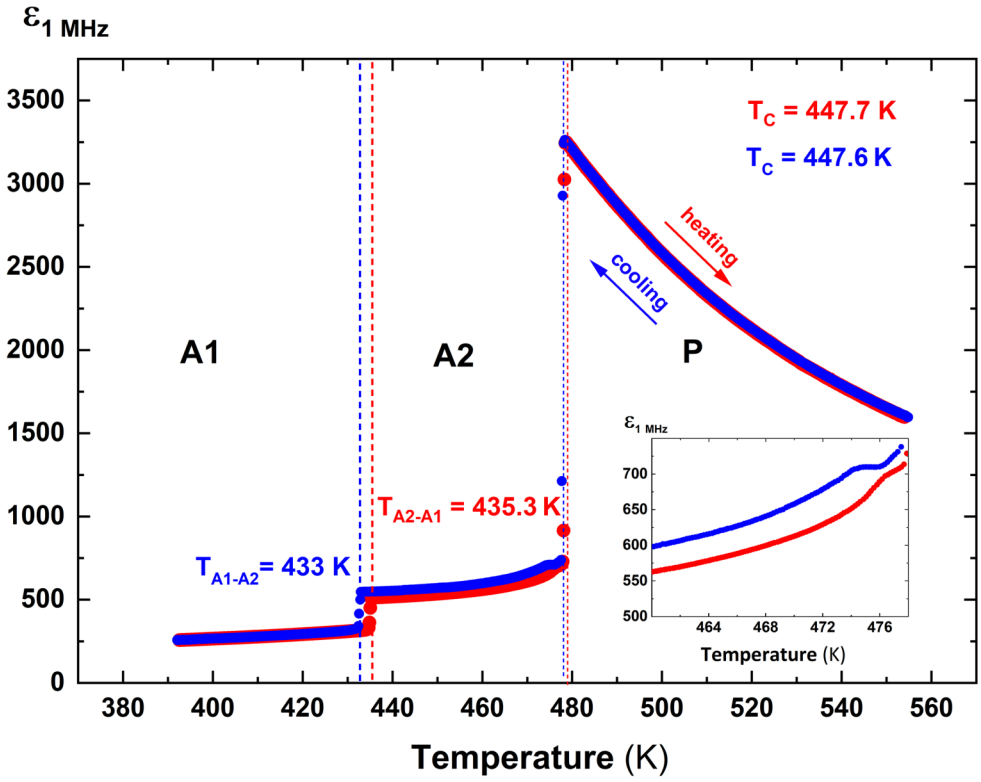


FIG. 6. Temperature dependence of the permittivity ε for $PbHfO_3$ single crystal. Phase transitions between the antiferroelectric A1 and A2, and paraelectric P are marked. The inset shows the permittivity anomaly below T_C, which is associated with the presence of DBs or ILMs; optical properties were investigated and are presented in Figs. 7–9 for PHO [Figs. 8(a) and 8(b)] and PZO [Figs. 9(a) and 9(b)].

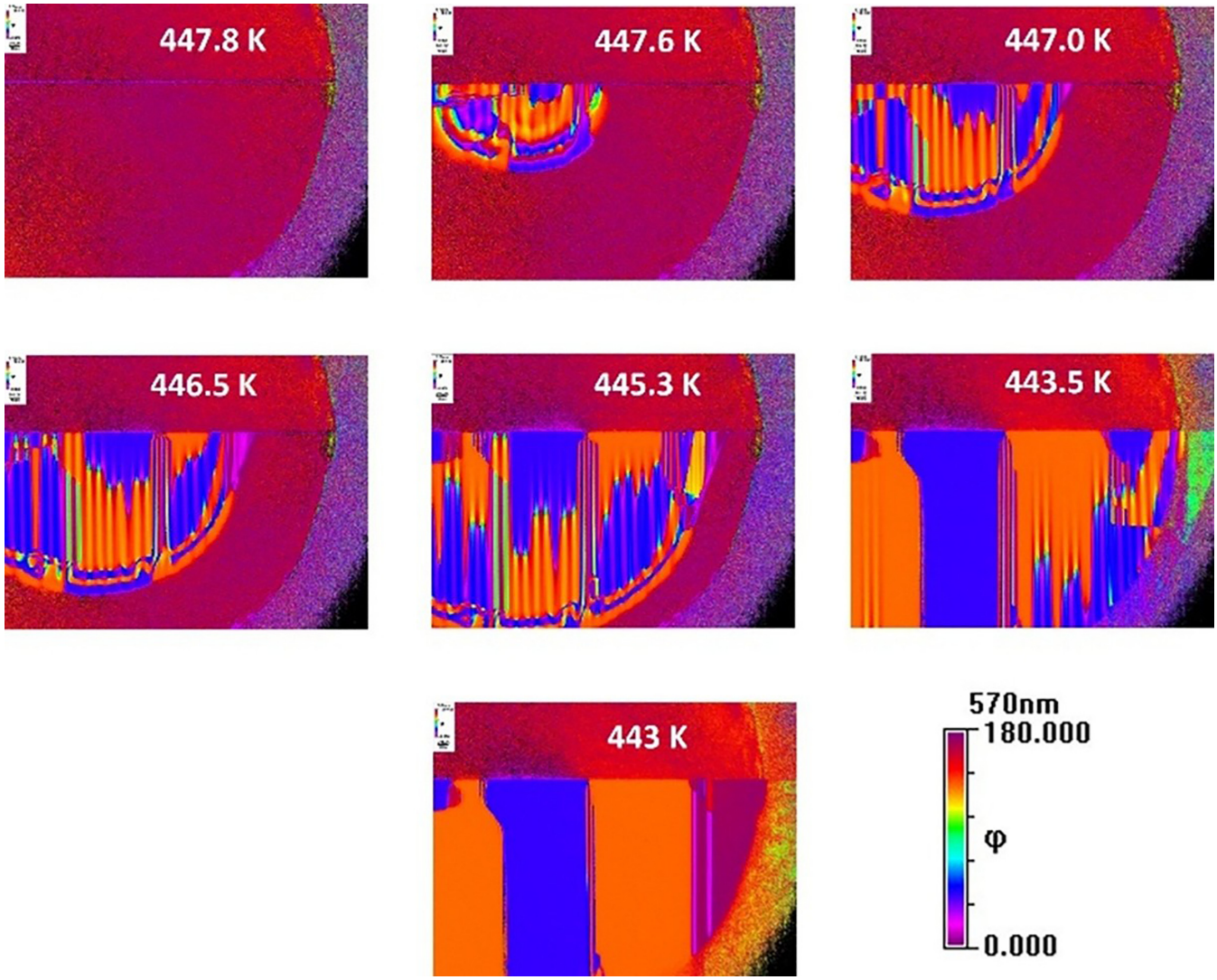


FIG. 7. Changes of the optical indicatrix orientation with temperature below $T_C = 447.7$ K for a single crystal of $PbHfO_3$, on cooling, according to the φ–colored label. The development of irregular-shaped regions within the intermediate phase between the P and A2 phases (see Fig. 6) is clearly visible. Finally, the crystal becomes antiferroelectric, characterized by large domains with linear domain boundaries (at 443 K).

measure of, e.g., co-existence of the phases (regions) of different symmetry.

IV. SUMMARY AND CONCLUSIONS

To summarize, we have shown that the mass of the polarizable subunit in lead transition metal perovskite oxides plays an essential role in their temperature-dependent soft modes, which follow the same dependence once mass-renormalized. This observation highlights their intrinsic similarities and emphasizes the role of their polarizability. This statement is in contrast to many theoretical assertions where the Pb ions are considered as the main drivers of the transition and where a two-order parameter ansatz is used to describe the properties of the Pb oxide perovskites [46]. These earlier approaches are based on the fact that the Pb ion lone pair configuration induces a hybridization with the oxygen ion p-states which is almost as strong as the transition metal oxygen hybridization. In addition, it causes an off-center shift of the lead ions, which reflects the shifts of the ferroelectric and antiferroelectric patterns of the transition metal oxygen displacements [47,48]. The lone pair can, however, not be at the origin of ferro-, antiferroelectricity since the remaining structural and electronic features are almost identical to $BaTiO_3$ where ferroelectricity originates from the interplay of the p-d covalent bonding, whereas the Ba ion is fully ionic [49]. In this or related work, the transient phase is not discussed in detail, which, in our opinion, is inherent and not caused by impurities or defects or dependent on the preparation method. We have put some emphasis on the TA modes related to PZO and PHO, which deviate from the overall temperature relation followed by the other modes, even when mass-renormalized, since these are crucial for the stability region of nonlinear solutions in terms of DB and ILM modes. Their momentum independence can be understood based on significant anharmonicity and nonlinearity, allowing for coexistence regimes of SPA, DB, and ILM modes. Additionally, they offer a microscopic explanation of precursor dynamics and the emergence

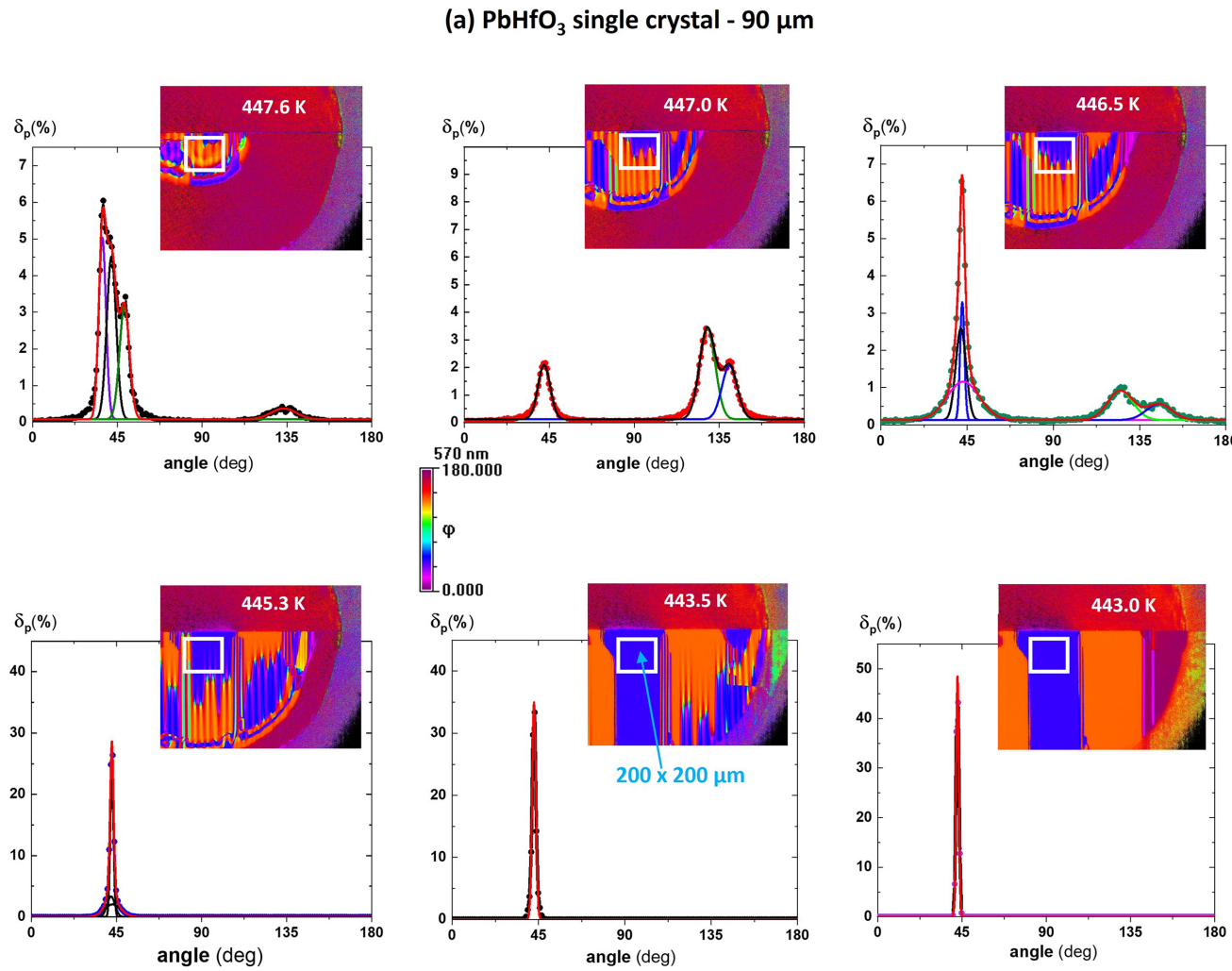


FIG. 8. (a) The Metripol technique enabled the calculation of the indicatrix orientation population δ_p in a well-defined region. In the upper Figure, we have chosen a region of 200 × 200 micrometres to observe changes in the indicatrix orientation inside the intermediate phase, which ultimately transforms into a large single domain (colored blue) with an orientation close to 45°, characteristic of orthorhombic symmetry. For each temperature point, the δ_p (deg) distribution has been fitted with a Lorentz function, better than a Gaussian, for processes with significant deviations from the average.

of the transient *ferroelectric-like* phase below T_C, as well as the challenging-to-resolve symmetry-related aspects. The formation of this transient phase, which is rarely addressed and poorly understood, is a typical signature of DB and ILM modes and can be experimentally investigated by examining mixed crystals of PZO, PHO, or PTO. For the series of PZO and PHO ($PbZr_{1-x}Ti_xO_3$), a related phase is observed on the PZO-rich side of the phase diagram ($x < 0.06$). Furthermore, ghost modes may serve as a signature, alongside relaxor-like properties, within the phase diagram. In thermodynamics, a broadening of the dielectric susceptibility and specific heat peaks is anticipated, caused by variations in the local double-well potential.

ACKNOWLEDGMENTS

The work was supported by the National Science Center, Poland, Grant No. 2022/47/B/ST3/02778. A.M. acknowledges the support of the UGB grant of ZFTK WAT for the year 2026.

DATA AVAILABILITY

There are no publicly available research data or software supporting this manuscript. Requests for further information or data should be sent to the authors.

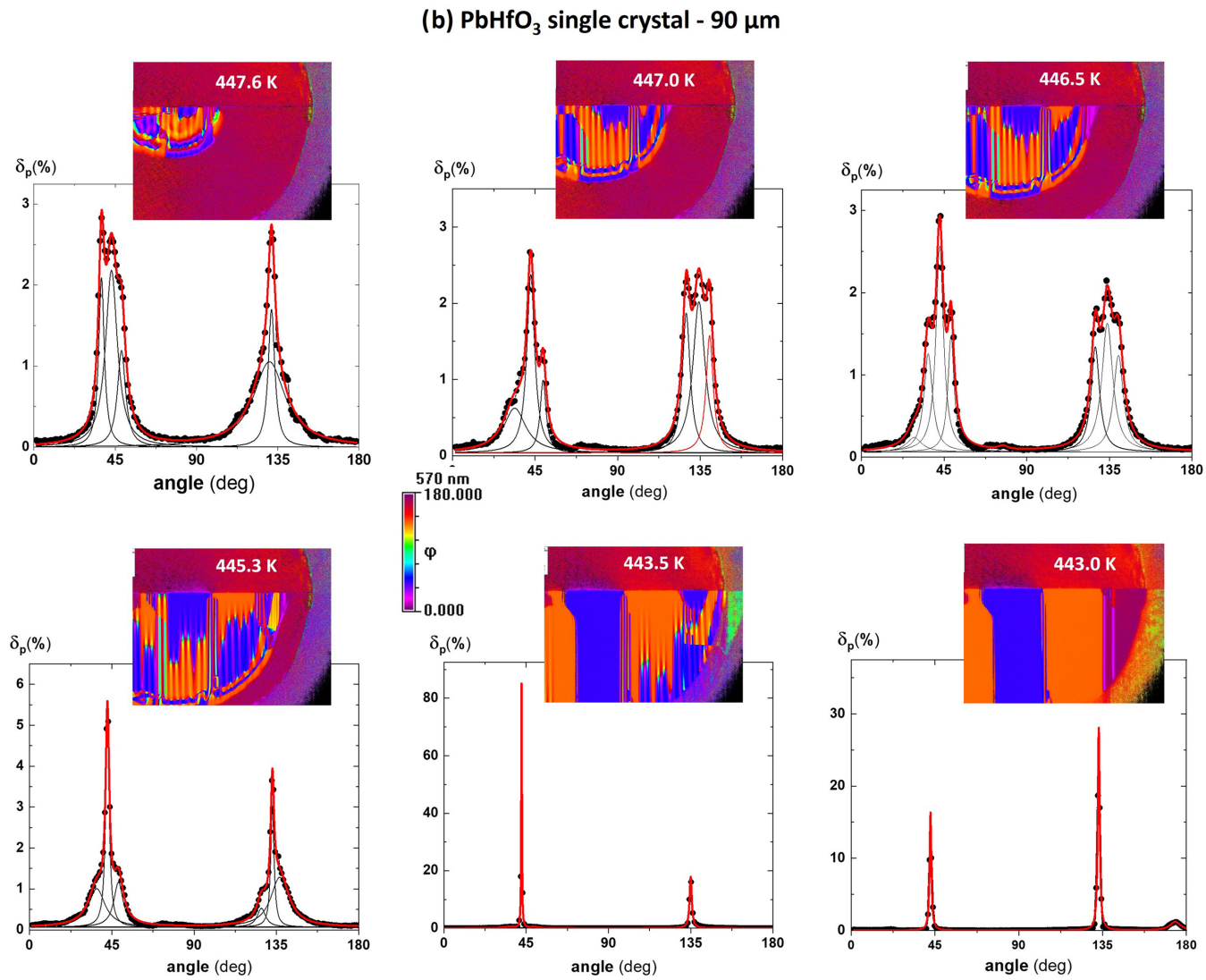


FIG. 8. (*Continued*) (b) Represents the δ_p (deg) changes for the entire intermediate region, which ultimately transform into three large domains (of blue and orange colors) with orientations close to 45° and 135°, both characteristic of the extinctions in orthorhombic symmetry. A small part of the crystal (the small peak at 443 K) transforms into the almost homogeneous domain of the 0° orientation, also permitted in the orthorhombic symmetry. Note that the maxima of the Lorentz functions lie between 0°−45° and 135°−180°, which are characteristic of monoclinic symmetry. The red line very well represents the cumulative effect of the subsequent Lorentz lines.

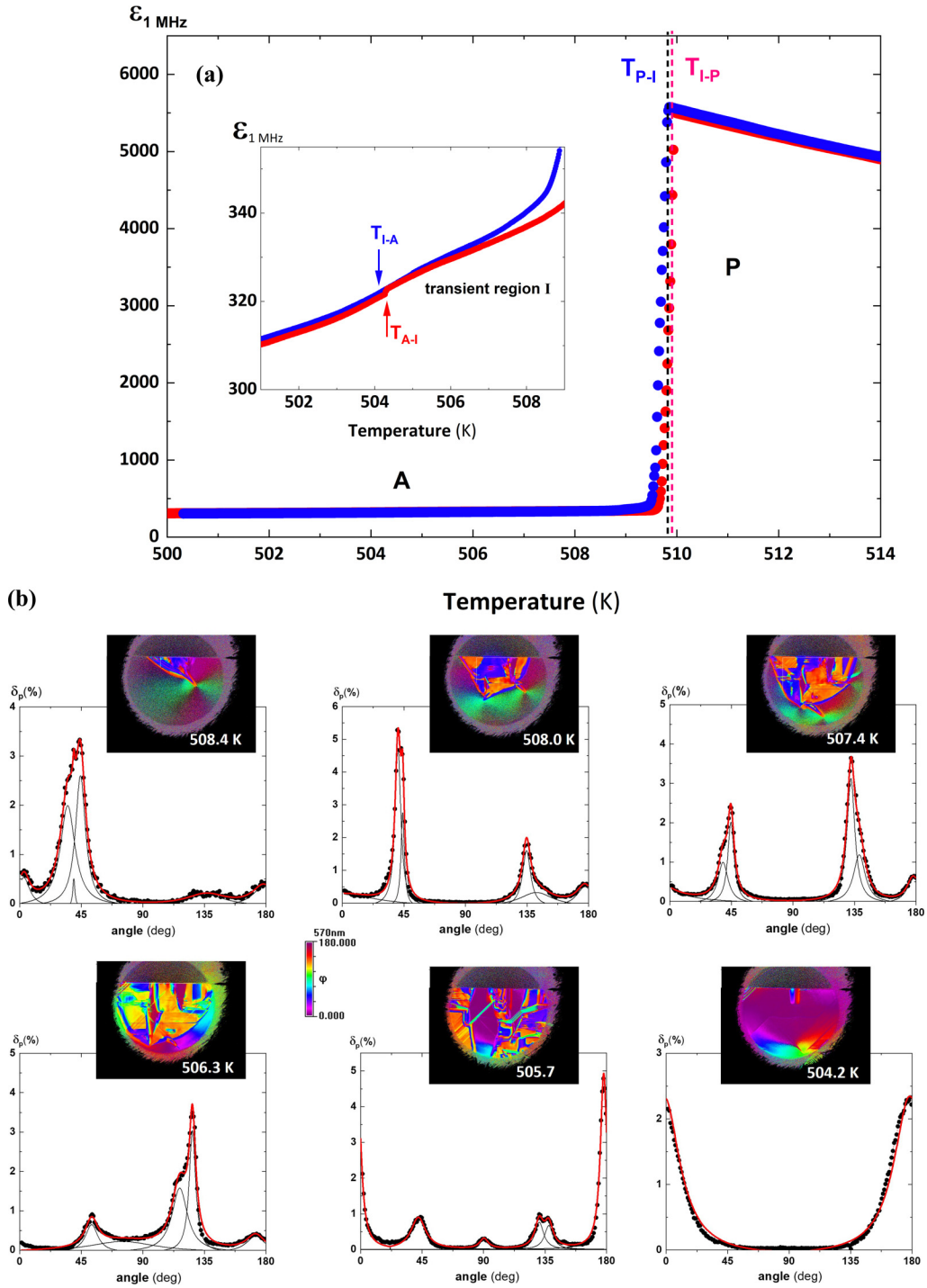


FIG. 9. (a) Temperature dependence of the permittivity for a single crystal of PZO of thickness 87 μm, on heating (red curve) and cooling (blue curve). Below T_C (T_{P-I}), the existence of the transient phase I between paraelectric P and antiferroelectric A is visible. The inset shows specific $\varepsilon(T)$ dependence inside the transient phase. (b) Similar to that in PHO, evolution of the inhomogeneous indicatrix orientations in the intermediate phase in the $PbZrO_3$ single crystal, on cooling. The δ_p (deg) relations were also fitted with Lorentz functions. As in the case of PHO, the maxima of the Lorentz functions lie between 0−45° and 135−180°, which is characteristic of the monoclinic symmetry.

[1] See e.g. the recent issue of F. Dogan, H. Lin, M. Guilloux-Viry, and O. Peña, Focus on properties and applications of perovskites, Sci. Technol. Adv. Mater. **16**, 020301 (2015).

[2] For a recent survey see: C. Li, H. Yu, T. Shu, *et al.*, PZT optical memristors, Nat. Commun. **16**, 6340 (2025).

[3] S. S. Cole and H. Espenschied, Lead titanate: Crystal structure, temperature of formation, and specific gravity data, J. Phys. Chem. **41**, 445 (1937); G. Shirane, and S. Hoshino, On the phase transition in lead titanate, J. Phys. Soc. Jpn. **6**, 265 (1951).

[4] G. Shirane and R. Pepinsky, Phase transitions in antiferroelectric $PbHfO_3$, Phys. Rev. **91**, 812 (1953).

[5] G. Shirane, E. Sawaguchi, and A. Takeda, On the phase transition in lead zirconate, Phys. Rev. B **80**, 485 (1950).

[6] C. Kittel, Theory of antiferroelectric crystals, Phys. Rev. **82**, 729 (1951).

[7] B. Ravel, N. Sicron, Y. Yacoby, E. A. Stern, F. Dogan, and J. J. Rehr, Order-disorder behavior in the phase transition of $PbTiO_3$, Ferroelectrics **164**, 265 (1995).

[8] K. Roleder, J. Handerek, Z. Ujma, and A. Kania, Problem of the transient phase between the paraelectric and the antiferroelectric phase in $PbZrO_3$, Ferroelectrics **70**, 181 (2011).

[9] V. J. Tennery, High-temperature phase transitions in $PbZrO_3$, J. Am. Ceram. Soc. **49**, 483 (1966).

[10] Z. Yu, N. Fan, Z. Fu, *et al.*, Room-temperature stabilizing strongly competing ferrielectric and antiferroelectric phases in $PbZrO_3$ by strain-mediated phase separation, Nat. Commun. **15**, 3438 (2024).

[11] X.-K. Wei, C.-L. Jia, H. Du, K. Roleder, J. Mayer, and R. E. Dunin-Borkowski, An unconventional transient phase with cycloidal order of polarization in energy-storage antiferroelectric $PbZrO_3$, Adv. Mater. **32**, 1907208 (2020).

[12] M. F. Kupriyanov, E. V. Petrovich, E. V. Dutova, *et al.*, Sequence of phase transitions in $PbHfO_3$, Crystallogr. Rep. **57**, 205 (2012).

[13] A. Bussmann-Holder, T. H. Byoung, W. L. Kim, K. Jae-Hyeon, A. Majchrowski, A. Soszyński, and K. Roleder, Phase transitionsand interrelated instabilities in $PbHfO_3$ single crystals, J. Phys. Condens. Matter **27**, 105901 (2015).

[14] A. Bussmann-Holder, M. Fiajłkowski, A. Majchrowski, A. Szewczyk, J. Więckowski, I. Lazar, A. Soszyński, and K. Roleder, Low-temperature polarity in antiferroelectric $PbZrO_3$ and $PbHfO_3$ driven by dynamical covalency in the ZrO_6 and HfO_6 substructures, Phys. Rev. B **112**, 174112 (2025).

[15] K. Roleder, A. Majchrowski, J. K. Zaręba, A. Bussmann-Holder, I. Lazar, I. Jankowska-Sumara, D. Kajewski, and A. Soszyński, Huge low-temperature polarity in the antiferroelectric $PbHfO_3$, Phys. Rev. B **111**, 214111 (2025).

[16] A. Bussmann-Holder, K. Roleder, and J-H. Ko, What makes the difference in perovskite titanates? J. Phys. Chem. Solids **117**, 148 (2018).

[17] A. Bussmann-Holder, J.-H. Ko, and K. Roleder, Chap. 3: The intricate lattice dynamics of perovskite oxides, OAJ Mater. Devices **5**, 1 (2020).

[18] H. Liu and B. Dkhil, A brief review on the model antiferroelectric $PbZrO_3$ perovskite-like material, Z. Kristallogr. Cryst. Mater. **226**, 163 (2011).

[19] K. Kurushima, H. Nakajima, T. Ogata, Y. Sakai, M. Azuma, and S. Mori, Relationship between Pb ion off-centering and lone pair electrons, Sci. Rep. **15**, 9314 (2025).

[20] D. Schütz and K. Reichmann, Complex bonding in perovskite ferroelectrisc, JCS Japan **122**, 231 (2014).

[21] R. Migoni, H. Bilz, and D. Bäuerle, Origin of Raman scattering and ferroelectricity in oxidic perovskites, Phys. Rev. Lett. **37**, 1155 (1976).

[22] H. Bilz, G. Benedek, and A. Bussmann-Holder, Theory of ferroelectricity: The polarizability model, Phys. Rev. B **35**, 4840 (1987).

[23] A. Bussmann-Holder, The polarizability model for ferroelectricity in perovskite oxides, J. Phys.: Condens. Matter **24**, 273202 (2012).

[24] A. Bussmann-Holder and H. Büttner, Ferroelectricity in oxides, Nature (London) **360**, 541 (1992).

[25] A. Bussmann-Holder, K. Roleder, and J.-H. Ko, Instabilities in the ferro- and antiferroelectric lead perovskites driven by transition metal ion mass: From $PbTiO_3$ via $PbZrO_3$ to $PbHfO_3$, J. Phys.: Condens. Matter **26**, 275402 (2014).

[26] A. Bussmann-Holder, H. Büttner, and A. R. Bishop, Polar-soft-mode-driven structural phase transition in $SrTiO_3$, Phys. Rev. Lett. **99**, 167603 (2007).

[27] J.-H. Ko, K. Roleder, A. Majchrowski, and A. Bussmann-Holder, Elastic anomalies associated with the antiferroelectric phase transitions of $PbHfO_3$ single crystals, J. Korean Phys. Soc. **64**, 1169 (2014).

[28] G. Shirane, J. D. Axe, J. Harada, and J. P. Remeika, Soft ferroelectric modes in lead titanate, Phys. Rev. B **2**, 155 (1970).

[29] I. Jankowska-Sumara, G. E. Kugel, K. Roleder, and J. Dec, Raman scattering in pure and Ti-doped $PbHfO_3$ antiferroelectric crystals, J. Phys.: Condens. Matter. **7**, 3957 (1995).

[30] J. Hlinka, T. Ostapchuk, E. Buixaderas, C. Kadlec, P. Kuzel, I. Gregora, J. Kroupa, M. Savonov, A. Klic, and J. Drahokoupil, Multiple soft-mode vibrations of lead zirconate, Phys. Rev. Lett. **112**, 197601 (2014).

[31] R. Burkovsky, G. I. Bronwald, D. Andronikova, G. Lityagin, J. Piecha, S.-M. Souliou, A. Majchrowski, A. Filimonov, A. Rudskoy, K. Roleder, A. Bosak, and A. Tagantsev, Triggered incommensurate transition in $PbHfO_3$, Phys. Rev. B **100**, 014107 (2019).

[32] L. Classen and J. J. Betouras, High-order van hove singularities and their connection to flat bands, Annu. Rev. Condens. Matter Phys. **16**, 229 (2025).

[33] H. Luo, L. Zhao, Z. Zhao, H. Yang, Y.-P. Huang, H. Liu, Y. Gu, F. Jin, and H. Chen, *et al.* Van Hove singularity driven emergence of multiple flat band-like nondispersive features in Kagome superconductors, Phys. Rev. B **111**, 155123 (2025).

[34] D. L. Corker, A. M. Glazer, W. Kaminski, R. W. Whatmore, J. Dec, and K. Roleder, Investigation into the crystal structure of the perovskite lead hafnate, $PbHfO_3$, Acta Cryst. B **54**, 18 (1998).

[35] S. Ren, H. X. Zong, X. F. Tao, *et al.*, Boson-peak-like anomaly caused by transverse phonon softening in strain glass, Nat. Commun. **12**, 5755 (2021).

[36] Z. Liu, L. Rui, M. Hao, C. Chai, J. Lu, Y. Gao, J. Shifeng, and X. Chen, Boson-peak-like anomaly induced by dipole disordered states in $(CH_3NH_3)_4InCl_7$, Phys. Rev. Lett. **133**, 216101 (2024).

[37] M. I. Klinger, Soft-mode related origin of the boson peak and acoustic-phonon broadening in glasses, Theor. Math. Phys. **154**, 64 (2008).

[38] A. Bussmann-Holder and A. R. Bishop, Inhomogeneity, local mode formation, and the breakdown of the Bloch theorem in complex charge transfer systems as a consequence of discrete breather formation, Phys. Rev. B **70**, 184303 (2004).

[39] A. J. Sievers and S. Takeno, Intrinsic localized modes in anharmonic crystals, Phys. Rev. Lett. **61**, 970 (1988).

[40] A. Hofstrand, H. Li, and M. I. Weinstein, Discrete breathers of nonlinear dimer lattices: Bridging the anti-continuous and continuous limits, J. Nonlinear Sci. **33**, 59 (2023).

[41] A. R. Bishop, A. Bussmann-Holder, S. Kamba, and M. Maglione, Common characteristics of displacive and relaxor ferroelectrics, Phys. Rev. B **81**, 064106 (2010).

[42] J. Macutkevic, J. Banys, A. Bussmann-Holder, and A. R. Bishop, Origin of polar nanoregions in relaxor ferroelectrics: Nonlinearity, discrete breather formation, and charge transfer, Phys. Rev. B **83**, 184301 (2011).

[43] A. Bussmann-Holder, A. R. Bishop, and T. Egami, Relaxor ferroelectrics and intrinsic inhomogeneity, Europhys. Lett. **71**, 249 (2005).

[44] K. Fujii, Introduction to the rotating wave approximation (RWA): Two coherent oscillations, J. Mod. Phys. **8**, 2042 (2017).

[45] I. Lazar, R. W. Whatmore, A. Majchrowski, A. Mike Glazer, D. Kajewski, J. Koperski, A. Soszyński, J. Piecha, B. Loska, and K. Roleder, Ultrahigh piezoelectric strains in $PbZr_{1-x}Ti_xO_3$ single crystals with controlled Ti content close to the tricritical point, Materials **15**, 6708 (2022).

[46] K. Patel, B. Xu, S. Prosandeev, R. Faye, B. Dkhil, P.-E. Janolin, and L. Bellaiche, Temperature-dependent properties of the antiferroelectric model $PbZrO_3$: An effective Hamiltonian study, Phys. Rev. B **106**, 214108 (2022).

[47] D. J. Singh, Structure and energetics of antiferroelectric $PrZrO_3$, Phys. Rev. B **52**, 12559 (1995).

[48] R. E. Cohen and H. Krakauer, Electronic structure studies of the differences in ferroelectric behavior of $BaTiO_3$ and $PbTiO_3$, Ferroelectrics **136**, 65 (1992).

[49] Ph. Ghosez, E. Cockayne, U. V. Waghmare, and K. M. Rabe, Lattice dynamics of $BaTiO_3$, $PbTiO_3$ and $PbZrO_3$: A comparative first-principles study, Phys. Rev. B **60**, 836 (1999).